Variability in porous ceramic fracture: influence of apparent density and critical pores

Julie Uhl, Sylvain Meille, Aurélien Doitrand

Variability in porous ceramic fracture : influence of apparent density and critical pores

Julie Uhl[a], Aurelien Doitrand[a,*], Sylvain Meille[a]

[a] *Univ Lyon, INSA Lyon, Université Claude Bernard Lyon 1, CNRS, MATEIS, UMR5510, 69621 Villeurbanne, France*

Abstract

Gypsum specimen failure under four-point bending is investigated both experimentally and numerically. The analysis accounts for the variation in specimen thickness (in a large range from 10 to 90 mm), in pore volume fraction (related to a variation in elastic and fracture properties) and for the presence of macropores that are likely to trigger failure. Examination of specimen fracture surfaces reveals several isolated macropores near the specimen face loaded under tension. The critical pore size does not depend on the specimen volume. The pore criticity does not only depends on its size but also on its location with respect to the specimen face sollicitated under tension. Both pore volume fraction variations between samples and the presence of critical pores induce failure stress scattering for a given specimen width, which is well reproduced numerically using the coupled criterion.

Keywords: Strength; porosity/flaw; Four-point bending; Coupled criterion ;

1. Introduction

The influence of the characteristic structure size on failure stress is generally referred to as "size effect". Two main points of view enable describing this size effect. The first explanation relies on the weakest link theory which is a statistical description of failure [1, 2, 3]. It is based on the assumption that failure occurs due to a critical flaw in an area sollicitated in tension. The second assumption states that the larger the specimen, the larger the probability to encounter a large critical flaw. Based on these assumptions, Weibull's approach describes the failure probability as a function of the maximum local stress level

*Corresponding author
Email address: aurelien.doitrand@insa-lyon.fr (Aurelien Doitrand)

and sample volume sollicitated under tensile loading. Even if these assumptions rely on mechanical considerations, this is an empirical statistical approach that is not based on a mechanical description of failure. This approach is frequently used for ceramic failure study [4, 5, 6] including porous ceramic failure assessment [7, 8].

The alternative viewpoint to explain size effects is based on a mechanical description of failure and the interaction between a characteristic length of the material and the structure characteristic dimensions. It was introduced by Bazant *et al.* [9, 10, 11, 12] who combined Linear Elastic Fracture Mechanics (LEFM) and the theory of plasticity to define the material characteristic length $E\mathcal{G}_c/((1-\nu^2)\sigma_y^2)$, where σ_y is the yield limit, E the material Young's modulus, ν the Poisson's ratio and $\mathcal{G}_c$ the critical energy release rate. LEFM studies the propagation of a pre-existing crack and thus cannot assess the initiation of a crack. This shortfall was overcome by the Coupled Criterion (CC) introduced by Leguillon [13]. The CC is based on the simultaneous fulfillment of stress and energy conditions which enables the determination of the initiation load and crack length [14, 15].

The CC is able to account for size effects such as, for instance, in composite materials [13, 16, 17, 18], in specimens with notches [19, 20, 21, 22] or holes [20, 22, 23, 24, 25, 26]. It was also recently extended to explain the large apparent failure stress obtained when studying nano- or micro-scale specimens [27, 28, 29, 30]. The CC was used in previous works first to study the bending strength variation as a function of the specimen width in elastic brittle materials such as gypsum [31]. The bending strength tends towards the tensile strength σ_c only if the specimen is large enough compared to the material characteristic length $l_{mat} = E\mathcal{G}_c/((1-\nu^2)\sigma_c^2)$, otherwise it increases as the specimen size decreases. Regardless of the material elastic and fracture properties, we highlighted the existence of a master curve describing the variation of the ratio of maximum flexural stress to tensile strength as a function of the specimen height to material characteristic length ratio. An analytical expression was derived which enabled the set-up of inverse identification procedure of both tensile strength and fracture toughness from bending tests. The influence of the specimen size on the failure stress was thus highlighted based on a mechanical analysis. The analysis presented in [31] enabled the determination of the failure force and therefore maximum stress under bending of specimens that do not contain any flaw. Then, we implemented the CC to evaluate

the influence of a critical flaw (*i.e.* a pore located in the area under tension) in gypsum specimen under bending [32]. It was shown that depending on the pore size and location within the specimen, crack initation may occur beyond the pore or in the pore to free surface ligament sollicitated under tension (starting either from the pore or from the free surface). For any pore size and location configurations, the CC enabled determining the failure force decrease compared to the reference configuration without pore. It was finally shown that several configurations may lead to the same failure force decrease, a larger pore further from the free surface being equivalent to a smaller pore closer to the free surface. These results questionned the assumption of Weibull's increasing critical flaw size with increasing specimen size since a smaller flaw may be more critical depending on its location. From this analysis, we determined for a given failure force decrease, all the admissible corresponding pore size and location couples. From experiments on gypsum specimens taken from [31], based on the admissible pore size/location couples, we inversely estimated the range of critical pore diameters, which lied around 50-250 μm. Interestingly, the pore size was found to be rather constant whatever the specimen size rather than decreasing as expected in Weibull's approach assumption. This result was obtained from inverse estimate based on failure forces and the CC, but no microscope observations were available to confirm these data.

The objectif of the present work is to study the influence of porosity on failure of gypsum specimen with different thicknesses under four-point bending. On one hand, it aims at evaluating the influence of the overall porosity fraction on failure due to mechanical property variations. On the other hand, it is dedicated to the experimental characterization of critical spherical macropores always present in gypsum samples and their influence on failure. Experiments are presented in Section 2. Macropore size and location characterization as well as fracture surface analysis are presented in Section 3. In Section 4, failure of four-point bending specimen is assessed using the CC considering the influence of critical pores.

2. Experiments

2.1. Experiment design

Previous works were dedicated to the comparison between Weibull's approach and the CC ability to reproduce experimentally observed size effects [32, 33]. The failure stress variation

as a function of specimen size could be studied and compared to experimental measurements, but no experiments with direct observations of the fracture surfaces were available. Weibull's approach assumes that the larger the specimen, the larger the critical flaw that causes failure whereas the CC is based on a mechanical reasoning that accounts for the actual size, location and shape of the flaw. We thus establish experiments in order to assess the assumption and results predicted by both models. We propose to test under four-point bending specimens having the same length and width, but with several thicknesses. From a theoretical point of view, it should enable assessing both approach assumptions and predictions. Indeed, since the specimen volume varies due to the thickness variation, Weibull's approach predicts that the critical flaw size should increase with increasing specimen volume, and therefore failure stress should decrease with increasing specimen volume. On the contrary, the CC will predict that in the absence of flaws, the same failure stress should be obtained whatever the specimen thickness since the same tensile stress gradient and energy release will be obtained whatever the specimen thickness. Of course, gypsum is a porous material thus we expect large pores in the specimens corresponding to entrapped air bubbles [34] which may act as critical flaws. Therefore, we need to quantify the pores shape, size and location to take it into account in the CC approach and to evaluate both model assumptions and predictions.

2.2. 4-points bending tests

The material under investigation is commercial β-gypsum. β-gypsum samples are prepared by hydration of β-hemihydrate at W/P=0.75 water to hemihydrate powder weight ratio. Rectangular specimens are prepared according to the following process:

- molds are cleaned and covered with demolding oil,
- water and hemihydrate powder are precisely weighted to respect the W/P ratio,
- powder is regularly added in water and followed by 30 s break,
- water and powder are spirally mixed until the paste is homogeneous,
- the paste is put into the mold and the paste surplus is removed by leveling,

- the specimen are unmolded after 30 minutes (the setting time is 15 minutes) and stored at 25°C during one week before the tests.

The temperature at which the tests are performed is 21$\pm$1 °C at 50$\pm$ 15% relative humidity. All tests are done in two consecutive days. The specimens all exhibit similar length (L = 100 $\pm$ 0.5 mm) and width (h = 9.7$\pm$0.7 mm) but different thicknesses: t=10 mm, 30 mm, 50 mm, 70 mm, or 90 mm. The specimen dimensions are summarized in Tab. 1.

Specimen type	1	2	3	4	5
t (mm)	10.2 $\pm$ 0.1	30.4 $\pm$ 0.3	50.4 $\pm$ 0.1	70.3 $\pm$ 0.2	90.4 $\pm$ 0.2
Number of specimens	7	7	7	7	6
h (mm)	9.65 $\pm$ 0.6	9.6 $\pm$ 0.5	9.6 $\pm$ 0.3	9.7 $\pm$ 0.4	9.8 $\pm$ 0.6
ρ (g/cm^3)	1.01 $\pm$ 0.04	1.05 $\pm$ 0.06	1.05 $\pm$ 0.02	1.06 $\pm$ 0.04	1.03 $\pm$ 0.03
F_c (N)	61.9 $\pm$ 13.0	161.1 $\pm$ 39.5	214.6 $\pm$ 40.0	303.6 $\pm$ 76.0	426.6 $\pm$ 83.0
σ_{max} (MPa)	4.1 $\pm$ 0.7	3.9 $\pm$ 0.7	3.1 $\pm$ 0.4	3.3 $\pm$ 0.9	3.2 $\pm$ 0.4

Table 1: Dimensions, failure force F_c and bending stress σ_{max}.

Four-points bending tests are performed on a Instron 8862 (USA) machine equipped with a 5 kN load cell at 0.5 mm/min displacement rate. The distance between lower supports is 75 mm and the distance between the upper supports is 29.5 mm. The specimen top face which was in contact with air during manufacturing in the mold is the most likely to present flaw or irregularities. Therefore, the specimen is placed in the four-point bending apparatus so that this face is sollicitated under compression. It is worth noting that the other faces do not present visible surface flaws. For all the specimens, a linear elastic behavior is recorded until brittle failure as typically noted for dry gypsum samples. The measured failure force F_c allows determining the corresponding failure stress $\sigma_{\max}$ from Euler-Bernoulli's beam theory (Tab. 1).

3. Results

3.1. Apparent density and mechanical property variation

Gypsum specimen apparent density depends on the amount of water and hemihydrate powder that is directly linked to the pore volume fraction inside the material. Fig. 1 depicts the apparent density variation as a function of specimen thickness. Relative variations up to 5% are noticed between the different specimens related to very small variations in W/P ratio.

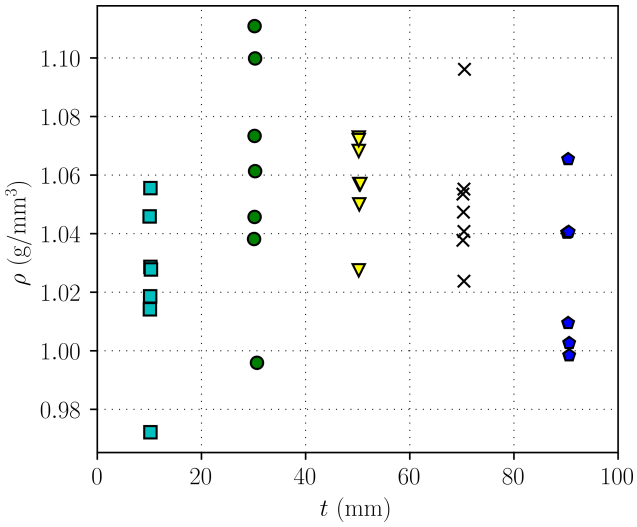

Figure 1: Specimen density variation as a function of specimen thickness.

Gypsum specimen apparent density has a first order influence on the mechanical properties [35, 36]. Actually, it is directly linked to the pore content in the specimen since the larger the pore volume fraction, the smaller the density. The relation between the pore volume fraction φ and the sample density ρ is given by:

$$\rho = \rho_0(1 - \varphi), \tag{1}$$

where $\rho_0 = 2.32$ is the pure gypsum specific gravity with no porosity. The variation in apparent density corresponds to pore volume fractions varying between 52 % and 58 % for the tested specimens. Pore volume fraction influence on gypsum mechanical properties (Young's modulus, tensile strength and critical stress intensity factor) was for instance studied by Meille [37], Meille and Garboczi [35], Sanahuja *et al.* [36] and Liu *et al.* [38]. From these works, we can derive the variation of the Young's modulus, tensile strength and critical energy release rate as a function of the pore volume fraction (Fig. 2). It was also shown in [35, 37] that the pore content variation induces a moderate variation of Poisson's ratio. From the density variations measured experimentally, we can derive variations on the pore volume fraction and thus deduce variations on the mechanical and fracture properties based on Fig. 2. It yields the following variations:

- Young's modulus between 2.8 GPa and 4.3 GPa,

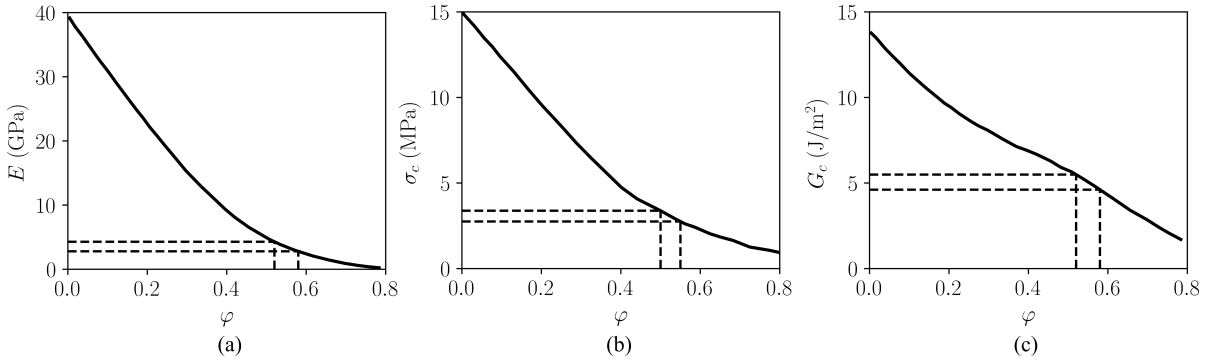

Figure 2: Young's modulus, tensile strength and critical energy release rate variations as a function of gypsum pore volume fraction [35, 36, 37].

- Tensile strength between 2.6 MPa and 3.4 MPa,
- Critical energy release rate between 4.6 J/m^2 and 5.5 J/m^2,

The influence of such property variations on numerical predictions of the failure stress under bending is studied in Section 4.2.

3.2. Fracture surfaces

Gypsum is obtained by mixing hemihydrate powder and water which results in entangled needle-shaped crystals formed by hydratation reaction. The porosity in the material consists in interconnected pores (micrometer size) between the gypsum crystals as well as some macropores (tens to hundreds of micrometers in diameter). The latter are due to the presence of entrapped air in the slurry, that will lead to macropores in the material after hydration and drying [34, 39]. Gypsum specimen fracture surfaces are observed using a magnifier in order to characterize the macropores (Fig. 3). Fracture surfaces were observed for all the tested specimens but only two specimens for each thickness are shown in Fig. 3 for the sake of clarity. Whatever the specimen thickness, spherical macropores are present on the fracture surface. Their diameter is in the order of magnitude of hundreds of micrometers. For most of the observed fracture surfaces, these macropores seem relatively far from one another. It seems that there is no preferential location for the pores on the fracture surface. A cluster of two or three macropores is also observed on few fracture surfaces. Almost no pores emerging at the surface under tension are observed on the fracture surfaces. In particular, no edge pores are observed on the specimen faces sollicitated under tension. These few edge pores

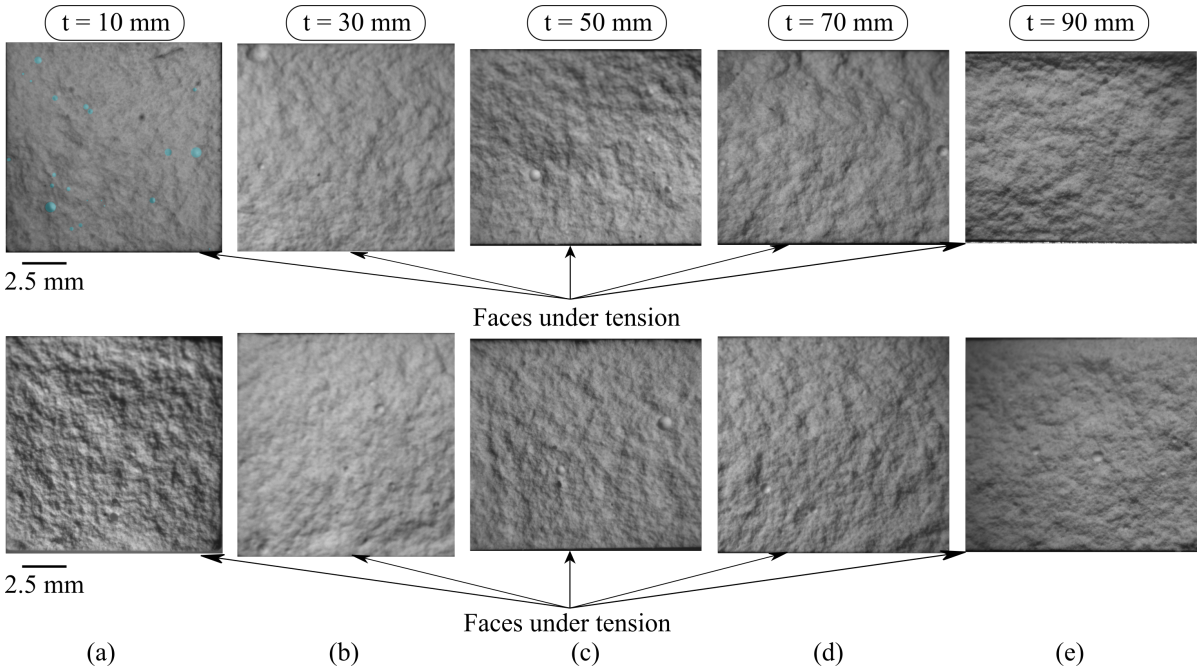

Figure 3: Fracture surfaces for specimen with different thicknesses (from two different specimens for a given thickness). Some pores are highlighted on the top left fracture surface.

are located on the specimen surface sollicitated under compression. Hydratation of hemihydrate powder with water is processed in a mold which means that the specimen top face is in contact with air. Edge pores are thus more likely to be observed on this face rather than other specimen faces since air bubbles entrapped in the slurry rather tend to move up to the top surface before setting. Macropores are likely to induce prematurate fracture provided they are large enough and located near the specimen surface sollicitated under tension [32]. For all tested specimens, we identify these critical pores and measure their diameter d and their distance to the specimen free surface h_d (Fig. 4). If several of these pores are observed on one fracture surface, we select the most critical based on the analysis given in [32]. Critical pore diameter and distance to the face under tension measurements for each sample are summarized in Table 2.

3.3. Porosity characterization and influence on failure stress

Fig. 5a shows the critical pore size as a function of specimen thickness. The mean critical pore size for a given specimen thickness lies between 0.3 mm and 0.4 mm for all the tested specimens without exhibiting an increasing trend with increasing specimen volume, as assumed in Weibull's approach. Indeed, it rather appears that the critical pore size lies

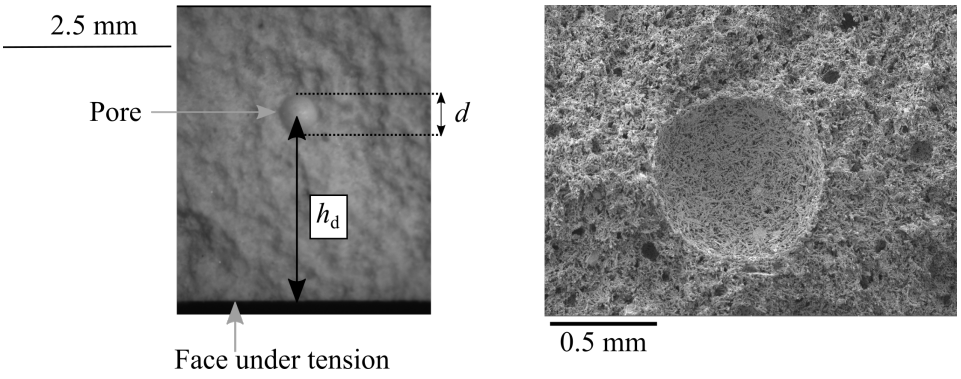

Figure 4: (Left) Focus on a critical pore and definition of its characteristics: distance to the specimen face under tension h_d and pore diameter d. (Right) SEM observation of a critical pore.

Type	1			2			3			4			5		
t (mm)	10.2 ± 0.1			30.4 ± 0.3			50.4 ± 0.1			70.3 ± 0.2			90.4 ± 0.2		
#	h_d	d	σ_{max}	h_d	d	σ_{max}	h_d	d	σ_{max}	h_d	d	σ_{max}	h_d	d	σ_{max}
1	0.29	0.28	4.7	0.35	0.19	3.3	0.64	0.21	2.9	0.32	0.28	4.1	0.84	0.24	2.0
2	2.10	0.42	4.0	0.43	0.32	3.3	1.43	0.33	3.2	0.33	0.39	2.6	0.2	0.3	3.4
3	0.27	0.37	3.5	0.63	0.32	4.7	0.28	0.36	2.8	1.74	0.15	3.2	2.97	0.46	2.9
4	0.67	0.27	4.8	0.54	0.45	3.9	0.68	0.28	3.3	0.74	0.26	3.8	1.34	0.68	2.8
5	2.06	0.52	3.6	0.59	0.18	3.8	0.49	0.17	2.9	0.82	0.27	2.4	0.37	0.27	3.6
6	0.29	0.3	4.3	0.43	0.22	3.6	3.2	0.58	2.7	1.03	0.83	2.5	0.12	0.18	2.8
7	1.59	0.42	4.2	0.4	0.5	3.8	0.75	0.20	3.5	0.3	0.55	2.9	N/A	N/A	N/A

Table 2: Critical pore center to free surface distance (h_d, in mm), pore diameter (d, in mm) and corresponding failure stress (σ_{max}, in MPa) measured from gypsum specimen fracture surface observations.

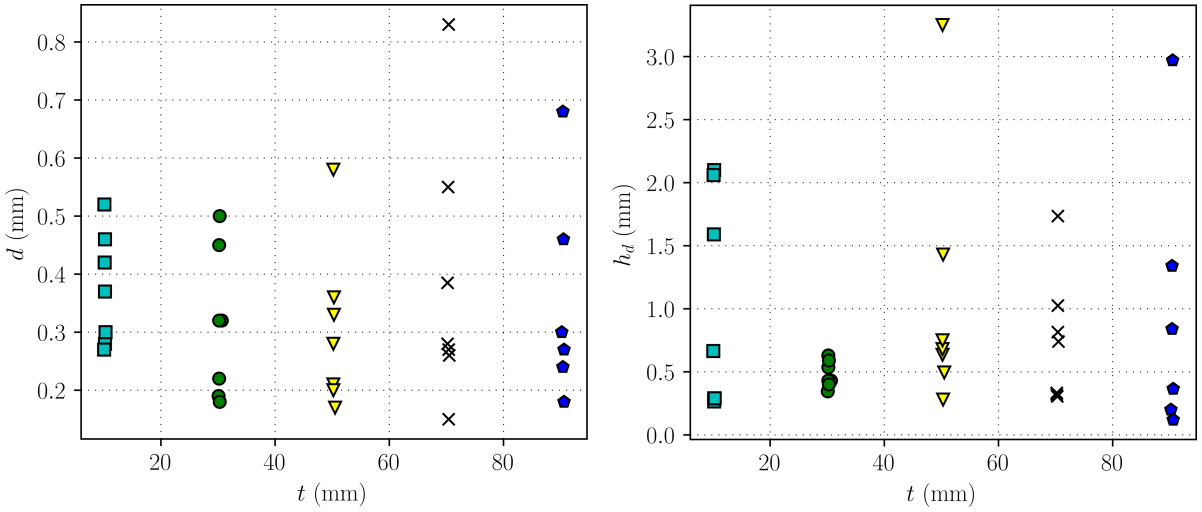

Figure 5: Pore a) diameter and b) distance to the specimen face under tension as a function of specimen thickness.

in the same order of magnitude whatever the specimen thickness and thus the specimen volume. This result is consistent with pore size variation as a function of specimen volume

obtained by inverse identification from other experiments on gypsum specimens [32]. This result can be explained by considering the processing, with dissolution of hemihydrate powder and subsequent precipitation of gypsum crystals. Macropores originate from air initially entrapped in the dry hemihydrate powder before mixing with water. The characteristics of these macropores in the final material are likely to be related to the rheology of the slurry during processing. Since the slurry rheology is controlled by the W/P ratio, similar for all samples, the characteristics of the macro porosity (number and diameter of pores) can be expected to be relatively similar for all the tested specimens. The pore distance to the specimen face under tension is shown in Fig. 5b. Most of the critical pores are located at less than 1.5 mm from the edge (*i.e.* approximately 1/7 of the specimen width), except for the smaller specimen series (thickness: 10 mm) for which three critical pores are located between 1.5 mm and 2.2 mm. One critical pore is also located between 1.5 mm and 3.5 mm away from the specimen face under tension for three other specimen series (with respective thickness: 50 mm, 70 mm and 90 mm). It can be noted that the criticity of a pore is not only linked to its size but also to its location with respect to the face under tension [32]. Fig. 6 shows the critical pore size and distance to free surface as a function of specimen pore volume fraction. First, it seems that there is no direct relation between the critical pore

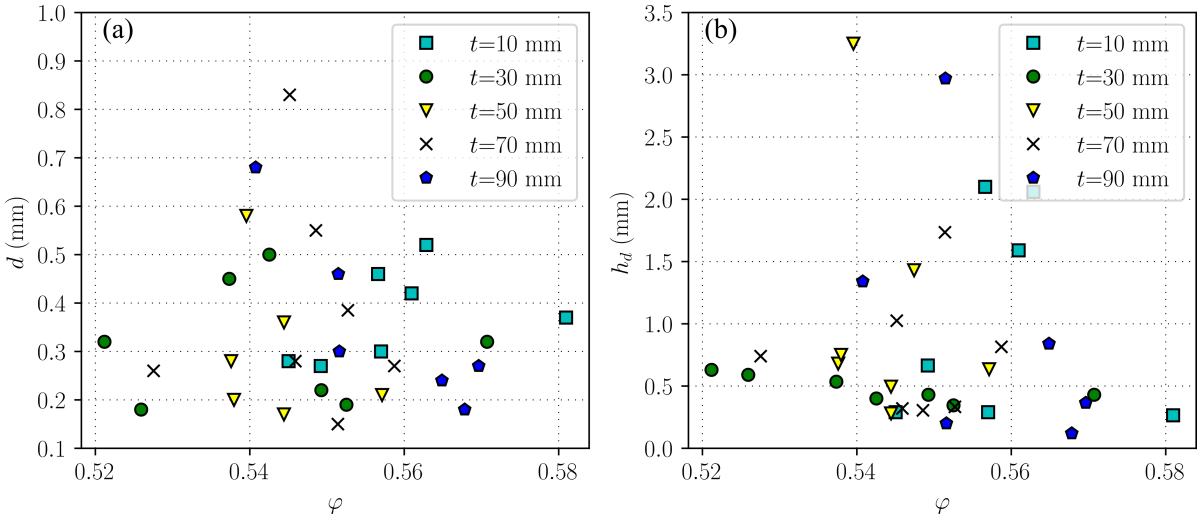

Figure 6: Pore a) diameter and b) distance to the specimen face under tension as a function of pore volume fraction.

size and the total pore volume fraction in the specimen (Fig. 6a). Indeed, the macropores only represent a very small fraction of the total porosity, the pore volume fraction is mainly

linked to the microporosity which does not vary much between all the samples. For a given specimen thickness, we observe a slightly decreasing trend of the critical pore distance to free surface as a function of the pore volume fraction even though the trend is not clearly observed for all the specimen sets.

Fig. 7 shows the variation of failure stress as a function of the specimen thickness. Seven specimens of each size may not be sufficient to observe a statistical effect and conduct

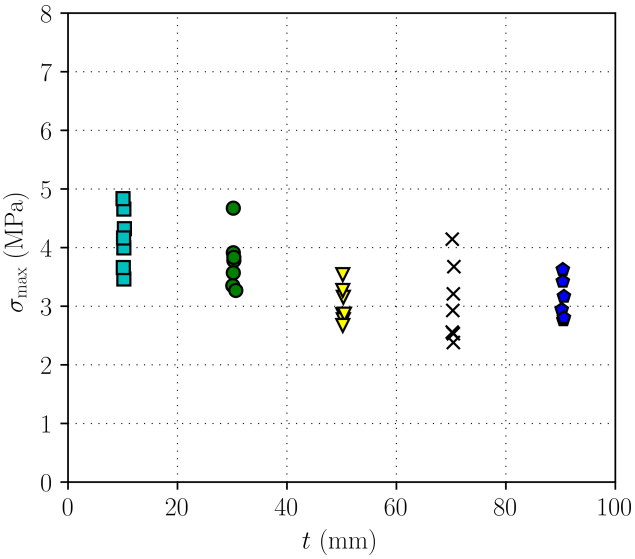

Figure 7: Failure stress as a function of specimen thickness obtained experimentally.

Weibull's model analysis, nevertheless it is sufficient to observe a failure stress scattering for a given specimen size. Indeed, for a given specimen thickness, stress variations are observed which may be explained by the specimen having different densities, widths and critical pore size and location. Apart from this source of variability, the failure stress is almost constant as a function of the specimen thickness. The mean failure stress value slightly increases for thicknesses smaller than 40 mm and remain constant for larger specimen thicknesses. Fig. 8 shows the failure stress variation as a function of the critical pore size and distance to the free surface. It is not straightforward to establish a clear trend between the failure stress and one of these parameters. From a theoretical point of view [32, 40], for a given distance to the specimen face under tension, a larger pore is expected to trigger failure at a smaller force and conversely, for a given pore size, the smaller the pore distance to free surface, the smaller the failure stress. Nevertheless, it is not made evident to observe this result from Fig. 8 since the data for a given pore size may not correspond to the same pore distance to free

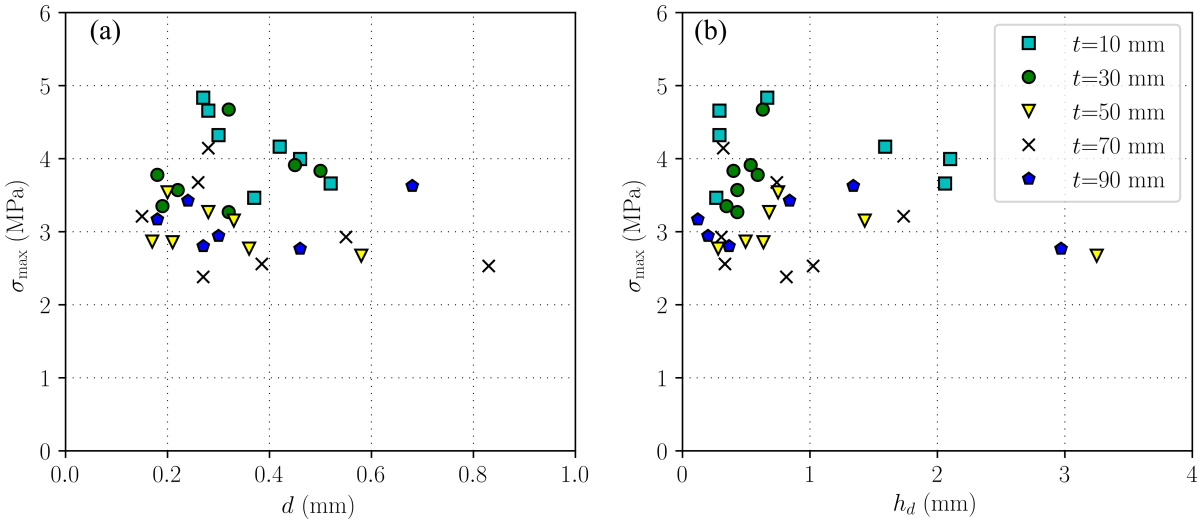

Figure 8: Failure stress as a function of pore a) diameter and b) distance to specimen face under tension obtained experimentally.

surface. Moreover, the different specimens also exhibit slightly different apparent densities and widths, both parameters having an influence on failure stresses.

The failure stress variation as a function of the specimen pore volume fraction is shown in Fig. 9. For a given specimen thickness, the failure stress exhibits a decreasing trend as a

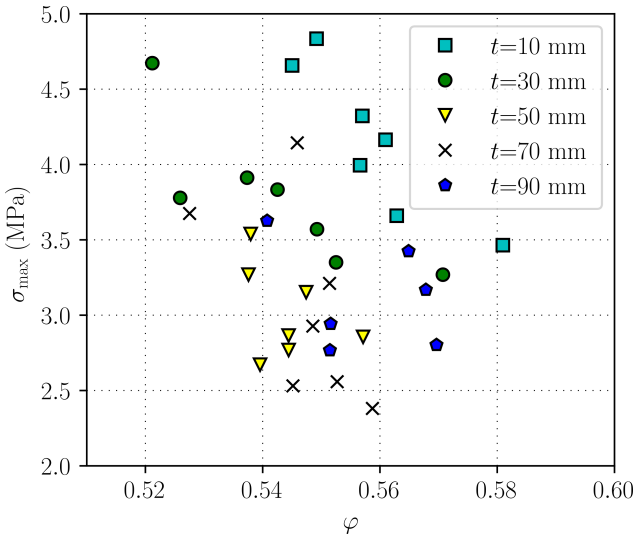

Figure 9: Failure stress as a function of pore volume fraction obtained experimentally.

function of the pore volume fraction. This variation can only partly be explained by higher mechanical and fracture properties corresponding to lower pore volume fraction (see Fig. 2) as the scatter for a given pore volume fraction seems related to the macropore characteristics.

4. Pore-induced failure modeling

In this section, we assess pore-induced failure using the numerical approach presented in [32], considering in addition the mechanical property variation as a function of the pore content. A brief recall of the CC is first presented. A more detailed presentation of the methodology so as to determine pore-induced crack initiation is also provided in [32].

4.1. The Coupled Criterion

Crack initiation assessment with the CC [13] consists in simultaneously fulfilling stress and energy conditions. The energy condition states that the potential energy variation before and after crack initiation is larger than the energy needed to nucleate the crack $\mathcal{G}_c \times S$ (where $\mathcal{G}_c$ is the material critical energy release rate and S the crack surface). The stress condition requires that prior to crack nucleation, the stress along the crack path is larger than the tensile strength σ_c. Under small deformation framework and linear elasticity assumption, the potential energy and the stress are respectively proportional to the square applied load and the applied load, which allows combining both conditions into a single equation that has to be solved in order to determine the initiation load level and crack extension [15]. The load level for crack initiation corresponds to the lowest value for which both energy and stress conditions are fulfilled. In practice, the stress and the potential energy are obtained by means of FE calculations corresponding to four-point bending specimen containing a critical pore [32] or not [31]. The proposed approach requires several input parameters, namely the specimen dimensions, the critical pore size and location in the specimen, the material elastic (Young's modulus, Poisson's ratio) and fracture (critical energy release rate, tensile strength) properties. Given these input parameters, the CC yields as ouptput the crack initiation force which also corresponds to the failure force for the problem under investigation.

4.2. Influence of input parameter variations

A first source of scattering is due to the specimens not having the exact same height, which varies from 9 mm to 10.4 mm. The influence of height variation on bending failure stress was already quantified in [31], it results in a ± 1 % relative variation in failure stress for given elastic and fracture properties. Another difficulty arising when studying gypsum is the

dependency on the elastic and fracture properties to the apparent density (or equivalently to the pore volume fraction). The studied specimens exhibit around ± 5 % variations in the pore volume fraction, which induces variations in elastic and fracture properties (see Fig. 2). We study the influence of such variations on failure stress variation in specimen without pore based on the analytical approach proposed in [31]. Fig. 10a shows the bending failure stress variation of gypsum specimens as a function of the pore volume fraction for a given $h = 10$ mm specimen width. Note that this result is obtained without considering the presence of a critical macropore, the variation is only due to elastic and fracture properties dependency on pore volume fraction. The pore volume fraction in the specimens under investigation varies between 52 % and 58 %, the parameters used in the CC are determined based on the specimen pore volume fraction using the data presented in Fig. 2. This variation in pore volume fraction and thus in elastic and fracture properties results in up to ± 10 % relative variation in failure stress. Therefore, the influence of the pore volume fraction on failure stress is much more pronounced than the influence of the specimen height.

Fig. 10b shows the failure stress as a function of the specimen thickness considering both actual pore volume fractions and sample widths. The variation in pore volume fraction and specimen width allows partly explaning the failure stress scattering measured experimentally.

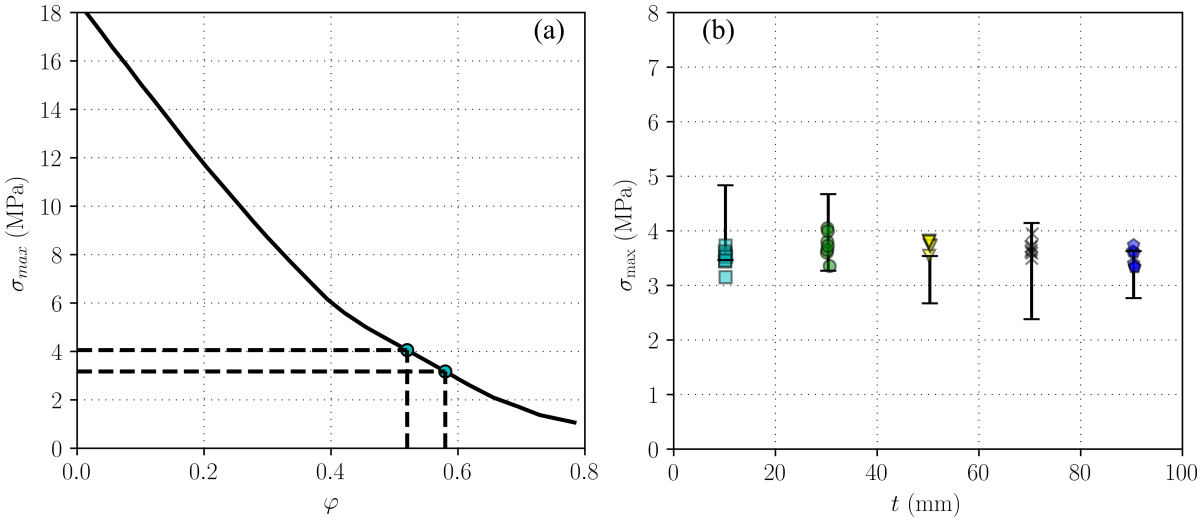

Figure 10: a) Failure stress variation of four-point bending specimen without critical pore as a function of pore volume fraction obtained with the CC for w=10 mm width. b) Failure stress as a function of specimen thickness obtained numerically (symbols) without considering the presence of a critical pore (range of values measured experimentally are also indicated as error bars).

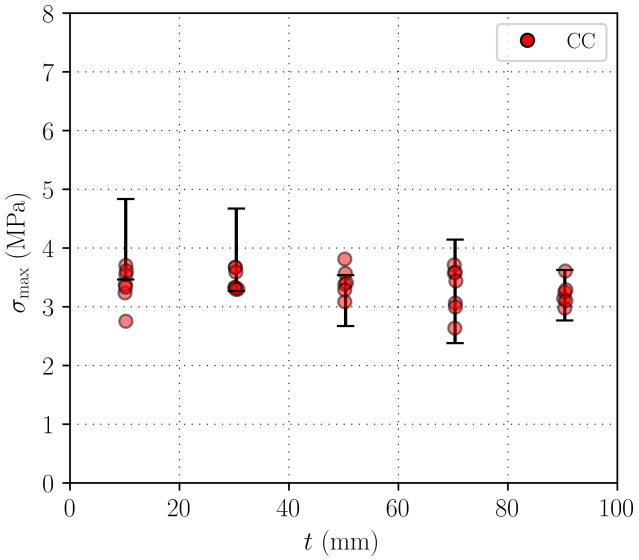

Figure 11: Failure stress as a function of specimen thickness obtained experimentally (error bars) and numerically using the CC accounting for density and width variation as well as the presence of a critical pore.

For a given specimen thickness, the obtained scattering lies between 26 % and 50 % of the scattering observed experimentally.

4.3. Pore-induced failure

We now compare the numerical predictions obtained with the coupled criterion to experimental results considering both apparent density variation and critical pore influence. Fig. 11 shows the failure stress variation as a function of the specimen thickness measured experimentally and obtained numerically with the CC considering the presence of a critical pore. The presence of a pore induces a decreases in the failure stress which can be calculated for all the specimens (Table 3). The failure force decrease induced by the presence of a pore varies up to 15.5% for all the studied specimens. It depends both on the pore diameter and location with respect to the specimen face under tension [32, 40]. The failure stress variation obtained using the coupled criterion is almost constant as a function of the specimen thickness. It enables reproducing similar scattering as obtained experimentally, except for 30 mm thickness specimen series for which the scattering obtained numerically represents around 30 % of the experimental scattering. The comparison between experimental and numerical results can be deepened by comparing the failure forces obtained with both approaches for each specimen (Fig. 12). An overall good agreement is obtained since most of the points are close to the bisector (which corresponds to a perfect match) in Fig. 12.

Type	1	2	3	4	5
t (mm)	10.2 $\pm$ 0.1	30.4 $\pm$ 0.3	50.4 $\pm$ 0.1	70.3 $\pm$ 0.2	90.4 $\pm$ 0.2
1	0.7	8.2	14.9	0.1	1.44
2	0.7	1.7	3.7	1.1	14.2
3	14.4	10.4	4.8	0.1	15.5
4	11.8	3.4	13.1	14.7	0.1
5	1.6	11.2	9.1	14.0	15.2
6	2.3	9.7	0.3	24.1	1.3
7	3.7	13.0	15.7	38.5	7.8

Table 3: Decrease (in %) in the failure stress due to the presence of a pore with respect to the same configuration without pore.

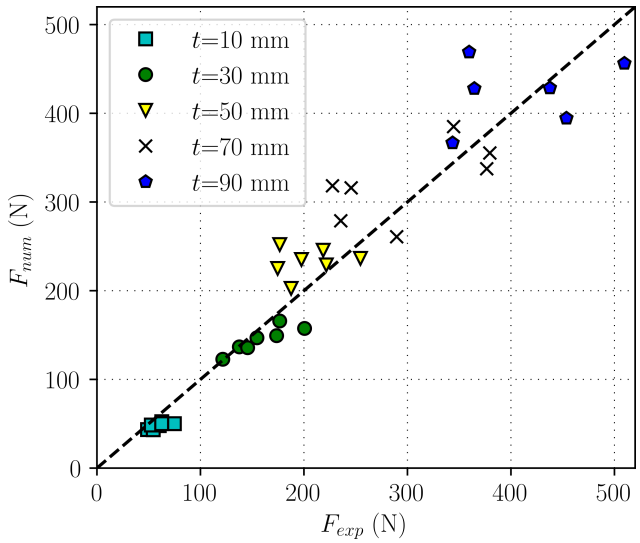

Figure 12: Failure force obtained numerically with the CC as a function of failure force measured experimentally.

4.4. Discussion

The experiments set-up in this work were initially motivated by a study of size effect in brittle fracture. They finally provide several conclusions regarding the use of the CC or Weibull's approach to assess such size effect.

First, it is worth noting that the variability in the failure stress is not only due to the presence of critical pores that induce prematurate failure. Indeed, for the specimen under investigation another source of variability is the variation in the pore content, which has a first order influence on macroscopic mechanical properties and thus on failure stress. This is an essential data that should be evaluated when using Weibull's approach for failure assessment. Since Weibull's modulus calculation mainly relies on failure stress scattering, all

sources of variability are taken into account in Weibull's approach. Therefore it is of primary importance to correctly identify the source of failure stress scattering in order to draw consistent conclusions and not directly relate it to variations in larger pore size. This result could explain some limitations about Weibull's model interpretation that were already noticed previously especially on porous materials [4, 32].

The CC enables considering the influence of the different sources of variability on failure stress, such as the variation in mechanical properties which yields failure stress variation range similar to those measured experimentally. The CC also enables the quantification of the influence of a critical pore on failure. For the specimen under investigation in this work, the failure stress decrease associated to the presence of a macropore lies around the same order of magnitude as the variation due to the influence of pore volume fraction. Therefore it is not straigthforward to identify the influence of such critical pores without considering the influence of the variation in the total pore content on the failure stress scattering. The method developped here could be applied to dense ceramics containing individual pores, thus avoiding the influence of fluctuation in total pore volume fraction. For instance, a prospective study would focus on dense ceramics with controled macro-defects possibly obtained using additive manufacturing. Finally, a limitation of the proposed approach applied to porous ceramics is the case where failure is induced by a cluster of pores, which has not be taken into account in the model and would require further developments.

5. Conclusion

Examination of the fracture surfaces of gypsum specimens tested in bending indicate the presence of several isolated critical macropores that are likely to trigger prematurate fracture. The critical pore size does not depend on specimen size whereas it is more likely to be located near the specimen face under tension for larger pore volume fractions. Pore criticity does not only depend on pore size but also on pore location with respect to the specimen face under tension. Two reasons mainly explain the failure stress scattering measured experimentally for a given specimen thickness, namely the variation in specimen pore volume fraction and the presence of critical pores triggering failure. Another source of variability comes from the variation in the specimen width. It may have a strong influence on the failure stress when

varying in a significant range and yield a mechanically-based explanation for experimentally observed size-effects [31]. However, in the present analysis, the specimen width variation is smaller than around 5% and induces an almost negligible variability on the failure stress in comparison to the two above-mentioned variability sources. Despite the failure stress scattering originating from both critical macropores and pore volume fraction variation, almost no size effect is observed when varying the specimen thickness (and thus increasing the specimen volume). The variation in pore volume fraction directly influences the material elastic and fracture properties. The presence of a pore induces a decrease in the failure stress depending on its location and size. Considering both pore volume fraction, critical pore presence and width variations, the CC enables the prediction of failure stress as a function of specimen thickness and allows accounting for the scattering measured experimentally. A good agreement is obtained between failure forces predicted by the CC and that measured experimentally.

References

[1] W. Weibull, The phenomenon of rupture in solids, Proc. Royal Swedish Inst. Eng. Res. 153 (1939) 1–55.

[2] W. Weibull, A statistical representation of fatigue failures in solids., Proc. Roy. Inst. Techn. 27 (1949).

[3] W. Weibull, A statistical distribution function of wide applicability, J. Appl. Mech. ASME 18 (1951).

[4] C. Lu, R. Danzer, F. Fischer, Scaling of fracture strength in ZnO: Effects of pore/grain size interaction and porosity, J. Eur. Cer. Soc. 24 (2004) 3643–3651.

[5] R. Danzer, R. Supancic, J. Pascual, T. Lube, Fracture statistics of ceramics - Weibull statistics and deviations from Weibull statistics, Engng. Fract. Mech. 74 (2007) 2919–2932.

[6] P. Bermejo, R. Supancic, R. Danzer, Influence of measurement uncertainties on the determination of the Weibull distribution, J. Eur. Cer. Soc. 32 (2012) 251–255.

[7] M. Genet, M. Houmard, S. Eslava, E. Saiz, A. Tomsia, A two-scale weibull approach to the failure of porous ceramic structures made by robocasting: Possibilities and limits, Journal of the European Ceramic Society 33 (4) (2013) 679–688.

[8] W. Lei, P. Zhang, Z. Yu, G. Qian, Statistics of ceramic strength: Use ordinary weibull distribution function or weibull statistical fracture theory?, Ceramics International 46 (13) (2020) 20751–20768.

[9] Z. Bažant, Size effect on structural strength: a review, Archive of applied Mechanics 69 (9-10) (1999) 703–725.

[10] Z. Bažant, Size effect in blunt fracture: concrete, rock, metal, ASCE J Engrg Mech 110 (1984) 518–35.

[11] Z. Bažant, P. Pfeiffer, Determination of fracture energy from size effect and brittleness number, ACI Materials J. 84 (1987) 463–480.

[12] Z. Bažant, Y. Xi, Statistical size effect in quasi-brittle structures: II. nonlocal theory, ASCE J. Eng. Mech. 117(11) (1991) 2623–2640.

[13] D. Leguillon, Strength or toughness? a criterion for crack onset at a notch, Eur. J. Mech. - A/Solids 21(1) (2002) 61–72.

[14] P. Weißgraeber, D. Leguillon, W. Becker, A review of finite fracture mechanics: crack initiation at singular and non-singular stress raisers, Archive Appl. Mech. 86(1-2) (2016) 375–401.

[15] A. Doitrand, E. Martin, D. Leguillon, Numerical implementation of the coupled criterion: Matched asymptotic and full finite element approaches, Fin. Elem. Anal. Des. 168 (2020) 103344.

[16] I. G. García, B. J. Carter, A. R. Ingraffea, V. Mantič, A numerical study of transverse cracking in cross-ply laminates by 3D finite fracture mechanics, Compos. Part B 95 (2016) 475–487.

[17] I. G. García, V. Mantič, A. Blázquez, The effect of residual thermal stresses on transverse cracking in cross-ply laminates: an application of the coupled criterion of the finite fracture mechanics, Int. J. Fract. 211 (2018) 61–74.

[18] I. García, J. Justo, A. Simon, V. Mantič, Experimental study of the size effect on transverse cracking in cross-ply laminates and comparison with the main theoretical models, Mech. of Mat. 128 (2019) 24–37.

[19] P. Cornetti, N. Pugno, A. Carpinteri, D. Taylor, Finite fracture mechanics: A coupled stress and energy failure criterion, Engng. Fract. Mech. 73 (2006) 2021–2033.

[20] D. Leguillon, D. Quesada, C. Putot, E. Martin, Size effects for crack initiation at blunt notches or cavities, Engng. Fract. Mech. 74 (2007) 2420–2436.

[21] A. Carpinteri, P. Cornetti, A. Sapora, Brittle failures at rounded V-notches: a finite fracture mechanics approach, Int. J. Fract. 172 (2011) 1–8.

[22] P. Cornetti, A. Sapora, A. Carpinteri, Mode mixity and size effect in V-notched structures, Int. J. Sol. Struct. 50(10) (2013) 1562–1582.

[23] A. Doitrand, R. Estevez, D. Leguillon, Experimental characterization and numerical modeling of crack initiation in rhombus hole pmma specimens under compression, Eur. J. Mech. Sol. 76 (2019) 290–299.

[24] E. Martin, D. Leguillon, N. Carrère, A coupled strength and toughness criterion for the prediction of the open hole tensile strength of a composite plate, Int. J. Sol. Struct. 49(26) (2012) 3915–3922.

[25] P. Cornetti, A. Sapora, Penny-shaped cracks by finite fracture mechanics, Int. J. Fract. 219 (2019) 153–159.

[26] A. Doitrand, A. Sapora, Nonlinear implementation of Finite Fracture Mechanics: A case study on notched Brazilian disk samples, Int. J. Non-Linear Mech. 119 (2020) 103245.

[27] A. Doitrand, R. Henry, J. Chevalier, S. Meille, Revisiting the strength of micron-scale ceramic platelets, J. Am. Cer. Soc. (2020). doi:10.1111/jace.17148.

[28] P. Gallo, A. Sapora, Brittle failure of nanoscale notched silicon cantilevers: a finite fracture mechanics approach, App. Sci. 10(5) (2020) 1640.

[29] A. Doitrand, R. Henry, I. Zacharie-Aubrun, G. J.M., S. Meille, UO_2 micron scale specimen fracture : Parameter identification and influence of porosities, Theor. Appl. Fract. Mech. 108 (2020) 102665.

[30] S. Jimenez Alfaro, D. Leguillon, Finite fracture mechanics at the micro-scale. Application to bending tests of micro cantilever beams., Engineering Fracture Mechanics (2021) 108012.

[31] A. Doitrand, R. Henry, S. Meille, Strength and fracture toughness estimation from four-point bending test, J. Theor. Comp. App. Mech. (2021). doi:https://doi.org/10.46298/jtcam.6753.

[32] A. Doitrand, R. Henry, T. Lube, S. Meille, Size effect assessment by weibull's approach and the coupled criterion, Engineering Fracture Mechanics 256 (2021) 107979. doi:https://doi.org/10.1016/j.engfracmech.2021.107979.

[33] D. Leguillon, E. Martin, M. Lafarie-Frenot, Flexural vs. tensile strength in brittle materials, Comptes Rendus Mecanique 343 (2015) 275–281.

[34] S. Meille, M. Saadaoui, P. Reynaud, G. Fantozzi, Mechanisms of crack propagation in dry plaster, J. Eur. Cer. Soc. 23 (2003) 3105–3112.

[35] S. Meille, E. Garboczi, Linear elastic properties of 2D and 3D models of porous materials made from elongated objects, Model. Simul. Mater. Sci. Engng. 9 (2001) 371–390.

[36] J. Sanahuja, L. Dormieux, S. Meille, C. Hellmich, A. Fritsch, Micromechanical explanation of elasticity and strength of gypsum: from elongated anisotropic crystals to isotropic porous polycrystals., J. Engng. Mech. 136 (2010) 239–253.

[37] S. Meille, Etude du comportement mécanique du plâtre pris en relation avec sa microstructure, Thèse de doctorat, Institut National des Sciences Appliquées de Lyon (2001).

[38] D. Liu, B. Savija, G. Smith, P. Flewitt, T. Lowe, E. Schlangen, Towards understanding the influence of porosity on mechanical and fracture behaviour of quasi-brittle materials: experiments and modelling, International Journal of Fracture 205 (2017) 57–72.

[39] J. Devillard, J. Adrien, S. Roux, S. Meille, E. Maire, Highlighting the role of heterogeneity on the indentation hardness of foamed gypsum, J. Eur. Cer. Soc. 40 (11) (2020) 3795–3805.

[40] A. Doitrand, D. Leguillon, Asymptotic analysis of pore crack initiation near a free edge, Theor. App. Fract. Mech. 116 (2021) 103125. doi:10.1016/j.tafmec.2021.103125.